Atmos. Chem. Phys., 18, 6661–6677, 2018
https://doi.org/10.5194/acp-18-6661-2018

Atmospheric Chemistry and Physics
Open Access
EGU

Photochemical aging of aerosol particles in different air masses arriving at Baengnyeong Island, Korea

Eunha Kang[1,5], Meehye Lee[1], William H. Brune[2], Taehyoung Lee[3], Taehyun Park[3], Joonyoung Ahn[4], and Xiaona Shang[1]

[1]Department of Earth and Environmental Sciences, Korea University, Republic of Korea
[2]Department of Meteorology, Pennsylvania State University, USA
[3]Department of Environmental Sciences, Hankuk University of Foreign Studies, Republic of Korea
[4]National Institute of Environmental Research, Republic of Korea
[5]Department of Urban and Environmental Studies, Suwon Research Institute, Republic of Korea

Correspondence: Meehye Lee (meehye@korea.ac.kr)

Received: 19 December 2016 – Discussion started: 2 January 2017
Revised: 17 March 2018 – Accepted: 23 March 2018 – Published: 9 May 2018

Abstract. Atmospheric aerosol particles are a serious health risk, especially in regions like East Asia. We investigated the photochemical aging of ambient aerosols using a potential aerosol mass (PAM) reactor at Baengnyeong Island in the Yellow Sea during 4–12 August 2011. The size distributions and chemical compositions of aerosol particles were measured alternately every 6 min from the ambient air or through the highly oxidizing environment of a potential aerosol mass (PAM) reactor. Particle size and chemical composition were measured by using the combination of a scanning mobility particle sizer (SMPS) and a high-resolution time-of-flight aerosol mass spectrometer (HR-ToF-AMS). Inside the PAM reactor, O_3 and OH levels were equivalent to 4.6 days of integrated OH exposure at typical atmospheric conditions. Two types of air masses were distinguished on the basis of the chemical composition and the degree of aging: air transported from China, which was more aged with a higher sulfate concentration and O : C ratio, and the air transported across the Korean Peninsula, which was less aged with more organics than sulfate and a lower O : C ratio. For both episodes, the particulate sulfate mass concentration increased in the 200–400 nm size range when sampled through the PAM reactor. A decrease in organics was responsible for the loss of mass concentration in 100–200 nm particles when sampled through the PAM reactor for the organics-dominated episode. This loss was especially evident for the m/z 43 component, which represents less oxidized organics. The m/z 44 component, which represents further oxidized organics, increased with a shift toward larger sizes for both episodes. It is not possible to quantify the maximum possible organic mass concentration for either episode because only one OH exposure of 4.6 days was used, but it is clear that SO_2 was a primary precursor of secondary aerosol in northeast Asia, especially during long-range transport from China. In addition, inorganic nitrate evaporated in the PAM reactor as sulfate was added to the particles. These results suggest that the chemical composition of aerosols and their degree of photochemical aging, particularly for organics, are also crucial in determining aerosol mass concentrations.

1 Introduction

In East Asia, atmospheric aerosols are a cause of public concern because of the frequent occurrence of haze in megacities and industrial areas, dust storms in deserts and extremely dry regions, and their transboundary transport (Takami et al., 2007; Wu et al., 2009; Kim et al., 2009; Ramana et al., 2010; Kang et al., 2013). These occurrences impact the regional air quality and climate (Li et al., 2011; Huang et al., 2014). Aerosol plumes are able to remain in the atmosphere for up to 10 days and can be transported across the Pacific Ocean. During transport, air masses become photochemically aged, leading to the generation of secondary aerosols and subsequent modification of the optical and microphysical properties of aerosols (Dunlea et al., 2009; Lim et al., 2014; Lee et

al., 2015). This transformation process has been studied by collecting ambient air across the Pacific Ocean and by tracking the Asian plumes onboard aircraft (Brock et al., 2004; Aggarwal and Kawamura, 2009; Dunlea et al., 2009; Peltier et al., 2008).

Secondary aerosols comprise inorganics, such as sulfate and nitrate, as well as organics. Of these, secondary organic aerosols (SOA) are of more interest because they are produced in the atmosphere from numerous organic species and are aged through complex mechanisms through which their physicochemical properties such as volatility, hygroscopicity, and optical properties are altered. The absorption and scattering properties of aerosols in northeast Asia were reported to be intimately linked with their chemical composition (Lim et al., 2014). As aerosols are oxidized, the hygroscopicity of organic aerosol (OA) increases, suggesting photochemically driven CCN activation of SOA (Massoli et al., 2010; Lambe et al., 2011; King et al., 2010; Morgan et al., 2010).

To understand SOA formation and aging processes, experiments have been conducted using environmental chambers (Kroll and Seinfeld, 2008; Hallquist et al., 2009). In these large environmental chambers, atmospheric simulations are limited to the equivalent of only about 1 day, which is much shorter than the nominal atmospheric lifetime of aerosols of about 1 week. In addition, ambient air masses are under the influence of various emissions and mixing processes, which are not properly represented in these well-mixed and long-residence-time chambers (Jimenez et al., 2009; Ng et al., 2010).

Thus, we introduced the potential aerosol mass (PAM) chamber, a continuous-flow reactor under high levels of OH and O_3 that is applicable for both controlled lab studies and ambient air (Cubison et al., 2011; Kang et al., 2007, 2011b; Lambe et al., 2012; Massoli et al., 2010). The highly oxidizing conditions of the PAM reactor are suitable for examining SOA formation and oxidation processes for the equivalent of 1 week or more (Jimenez et al., 2009; George and Abbatt, 2010). In particular, the PAM reactor has less wall loss mainly due to a much shorter residence time compared to conventional chambers. Thus, the PAM reactor is able to reasonably simulate the aging processes of SOA after formation (Kang et al., 2011a). In the first field deployment of PAM in northeast Asia, Kang et al. (2011a) reported PAM simulation results for different air masses and demonstrated that oxidation processes occurring in the natural atmosphere were plausibly integrated in the PAM reactor. Recently, a PAM reactor has been used to examine secondary aerosol formation and evolution from ambient air masses (Hu et al., 2016; Ortega et al., 2016; Palm et al., 2016) and emission sources (Ortega et al., 2013; Link et al., 2017; Timonen et al., 2017). The wall losses of aerosols and condensable gases and photochemistry of the PAM reactors have been studied to quantitatively understand the experimental results of the PAM reactor (Lamb et al., 2015; Palm et al., 2016, 2017; Peng et al., 2015, 2016).

In this study, we deployed a PAM reactor at an island site in the Yellow Sea to investigate the photochemical aging of ambient aerosols in sulfate-dominated northeast Asia. The particle size, mass, and chemical characteristics of ambient and PAM-processed aerosols were compared for different air masses transported from nearby continents. Their aging characteristics were examined in terms of secondary aerosol formation and the evolution of preexisting aerosol particles. The discussion mainly focused on the formation of sulfate and further oxidized organics and the loss of less oxidized organics upon photochemical oxidation in the PAM reactor.

2 Experimental methods

Experiments were conducted at a measurement station on Baengnyeong Island in the Yellow Sea (37.967° N, 124.630° E; 100 m a.s.l.) from 4 to 12 August 2011 (Fig. 1a). As the northernmost and westernmost part of South Korea, Baengnyeong Island is located 740 km west of Beijing and 211 km east of Seoul. The measurement station was established by the National Institute of Environmental Research (NIER) as a core background site of the National Monitoring Network to observe dust and pollution plumes transported from China. In previous studies conducted at the same site, sulfate and organic aerosols were enhanced under the influence of pollution plumes transported from eastern China and the Korean Peninsula (Choi et al., 2016; Lee et al., 2015).

Ambient air sampled using a $PM_{2.5}$ cyclone was pulled through a tubing (1 cm in diameter) into the PAM reactor for 6 min, during which the ambient aerosols were oxidized (hereafter referred to as "PAM aerosols"). For another 6 min, the sampled ambient air was directly pumped into the analytical instruments, bypassing the PAM reactor. The ambient and PAM aerosols were alternately measured every 6 min, thereby producing pseudo-simultaneous measurements.

The PAM reactor employed in this study is the same version as that described in Lambe et al. (2011), which was also used for laboratory studies of SOA aging (Lambe et al., 2012, 2015; Fig. S1). The ambient air was introduced into the PAM reactor through a SilcoNert-coated (SilcoTek, Inc.) inlet plate and endcap and then rapidly dispersed before entering the reactor through a SilcoNert-coated stainless-steel screen. For aerosol sampling, copper or stainless steel 1/4 inch OD tubes were used to minimize the particle loss on the tubing walls. The 1/4 inch PTFE Teflon tubes were used for the bypass flow. The total flow rate through both ambient sampling and the PAM reactor was 5 L min^{-1}. The flow in the PAM reactor was laminar (Reynolds number < 50), and aerosols were sampled at the center line. The residence time of air in the PAM reactor was 100 s based on flow rate and the volume of the reactor. During the experiment, the loss associated with the PAM reactor and inlet was determined. The SO_2 loss through a cyclone and inlet plate was 11 ± 7 % and aerosol particle

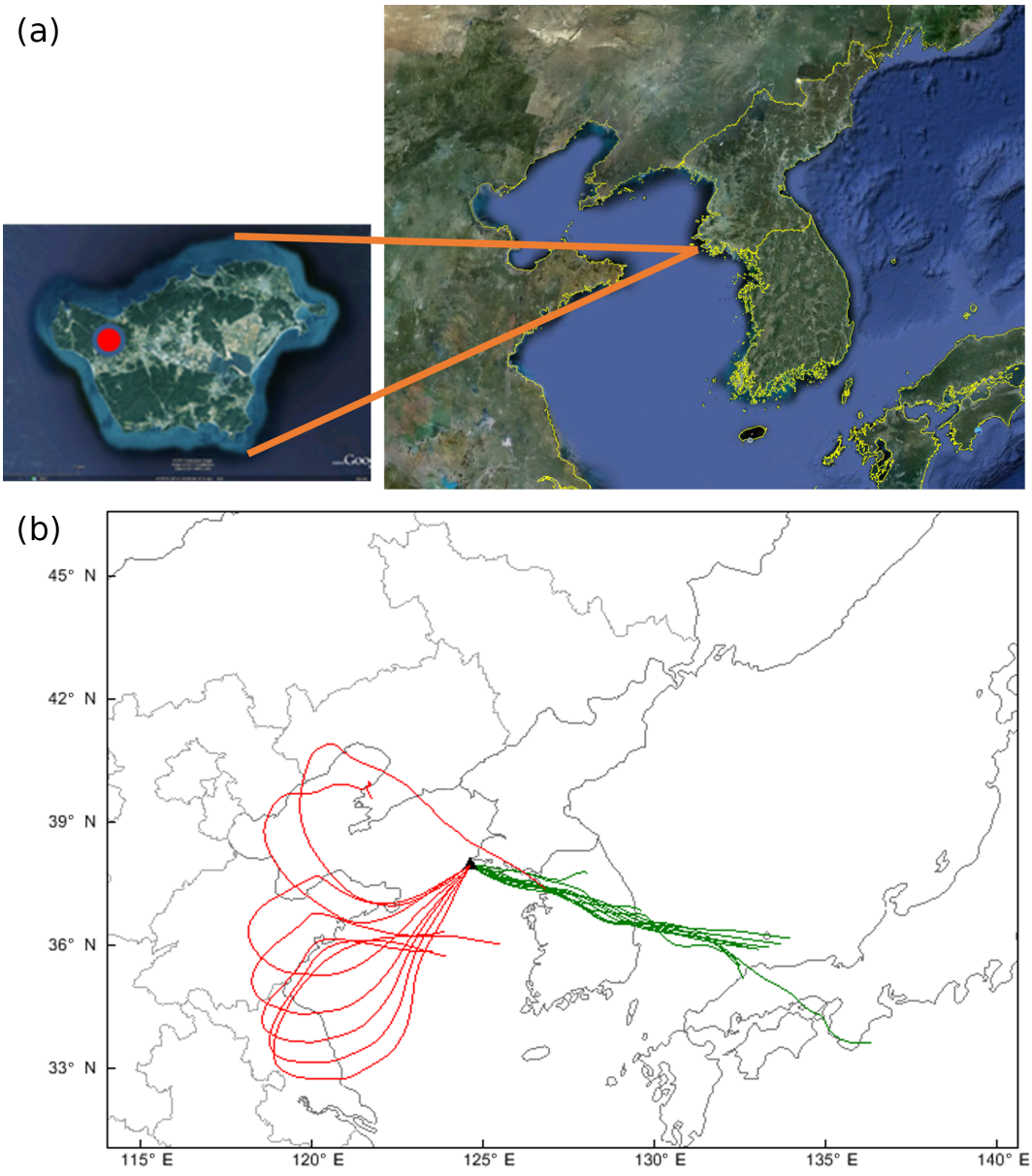

Figure 1. (a) The location of the measurement site on Baengnyeong Island, the northernmost island in South Korea. The red circle indicates the measurement station location. **(b)** 72 h backward trajectory for the two episodes. Green represents the organics-dominated episode during 6 August 11:00 LT to 7 August 2011 09:00 LT, while red represents the sulfate-dominated episode during 9 August 01:00 LT to 9 August 2011 14:00 LT

loss in the PAM reactor was about 12 % (Figs. S2-1 and S2-2 in the Supplement). The loss of particles and SO_2 gas was measured as the difference in concentration between ambient air and air pulled through the PAM reactor with UV lights off. In addition, the three-way switching valve might cause the evaporation of ambient and PAM aerosols when it gets hot during operation.

The PAM reactor is equipped with 30 cm long Hg lamps emitting 185 and 254 nm of light (82-9304-03, BHK Inc.) in order to produce large amounts of OH and O_3, creating a highly oxidizing environment (Fig. S1 in the Supplement). The UV lamps were housed in Teflon sleeves being purged by nitrogen with a flow rate of $\sim$ 50 sccm to prevent O_3 from building up inside the sleeves. This flow also slightly lowers the amount of heat being transferred from the lamps to the air in the chamber. The results of Ortega et al. (2016) using a PAM reactor the same as that used in the present study demonstrated that temperature increased by about 2 °C inside the PAM reactor. In a recent discussion, a 10 °C difference between PAM and ambient air caused the evaporation of inorganic nitrate up to 34 % and OA up to 25 % (https://docs.google.com/viewer?a=v&pid=sites&srcid=).

Table 1. Meteorological parameters and measurement summary for organics-dominated and sulfate-dominated episodes.

	Organics-dominated 6 Aug 11:00 LT ~ 7 Aug 09:00 LT		Sulfate-dominated 9 Aug 01:00 LT ~ 9 Aug 14:00 LT	
Meteorological parameters				
Temp (°C)	26 ± 0.8		20 ± 0.6	
Relative humidity (%)	84 ± 7.7		96 ± 0.2	
Wind speed ($m\,s^{-1}$)	5 ± 1.6		8 ± 1.7	
Wind direction	Easterly		Southwesterly	
Weather mark	Cloudy		Fog	
Gaseous species				
SO_2 (ppbv)	3.1 ± 0.3		3.4 ± 0.2	
NO_2 (ppbv)	2.4 ± 0.8		0.9 ± 0.3	
CO (ppmv)	0.2 ± 0.0		0.4 ± 0.1	
O_3 (ppbv)	46 ± 22		54 ± 8	
SMPS particle mass concentration[a]				
	Ambient	PAM	Ambient	PAM
Total mass conc.	14.04 ± 4.49	17.96 ± 5.66	25.00 ± 6.41	23.44 ± 8.91
$10 \sim 50$ nm	0.03 ± 0.03	0.73 ± 0.33	0.01 ± 0.01	0.29 ± 0.12
$50 \sim 200$ nm	5.55 ± 2.33	5.21 ± 2.19	7.78 ± 2.01	9.53 ± 2.54
$200 \sim 500$ nm	8.45 ± 2.27	12.03 ± 3.47	17.21 ± 5.49	13.62 ± 8.09
AMS particle mass concentrations[b]				
Sulfate	2.95 ± 1.31	4.59 ± 1.91	11.45 ± 4.65	14.66 ± 5.01
Nitrate	1.16 ± 0.85	0.52 ± 0.22	1.56 ± 1.01	0.45 ± 0.20
Ammonium	1.03 ± 0.62	1.51 ± 0.67	3.44 ± 1.36	4.07 ± 1.48
Organics	10.59 ± 3.71	7.97 ± 2.66	5.34 ± 1.85	3.84 ± 1.00
m/z 43	0.66 ± 0.04	0.31 ± 0.01	0.24 ± 0.02	0.10 ± 0.02
m/z 44	1.47 ± 0.08	1.91 ± 0.01	0.93 ± 0.06	0.98 ± 0.05

[a] SMPS particle mass concentrations were obtained from SMPS measurements corrected with a particle density of $1.4\,g\,cm^{-3}$, and units are $\mu g\,m^{-3}$.
[b] AMS particle mass concentrations of sulfate, nitrate, ammonium, and organics were obtained from MS-mode AMS measurements, and units are $\mu g\,m^{-3}$.

However, the ambient temperatures were $20 \sim 26\,°C$, which equaled or exceeded the temperature of the air-conditioned laboratory set to 20 °C. As a result, the temperature difference between the PAM reactor and the ambient air was at most a few degrees. Thus, temperature-induced evaporation of OA or nitrate in the PAM reactor would likely have been small.

In this study, the OH exposure of the PAM reactor was dependent on the humidity of the ambient air but not modulated by UV lamps. The exposure was originally set to 3–4 days for springtime to get the near-maximum mass concentration. However, the experiment was delayed by logistic problems and the OH exposure was closer to 4.6 days due to high humidity in summer.

The OH exposure of the PAM reactor was estimated to be 7×10^{11} molecules cm^{-3} s against sulfur dioxide decay in a study conducted by Kang et al. (2011b; Fig. S3-1 in the Supplement). When corrected for calculated OH suppression, it was 25 % lower than from the SO_2 calibration and was equivalent to an integrated OH concentration over 4.6 days at a typical noontime concentration of 1.5×10^6 molecules cm^{-3} (Mao et al., 2010). The OH suppression from VOCs and other OH-reactive gases were calculated using the oxidation chemistry model (Peng et al., 2016) with $30\,s^{-1}$ of external OH reactivity, representing rural areas (Feiner et al., 2016; Lee et al., 2009; Peng et al., 2016; Yoshino et al., 2006). Using this OH exposure, the calculated sulfate production matches the measured sulfate increase in the PAM reactor to within 16 % (Fig. S4-1 in the Supplement).

The chemical composition of the aerosol particles was measured by a high-resolution time-of-flight aerosol mass spectrometer (HR-ToF-AMS, hereafter referred to as AMS). The number concentration was determined in the mobility diameter range of 10.4–469.8 nm with a scanning mobility particle sizer (SMPS 3034, TSI; Jayne et al., 2000; Jimenez et al., 2009; DeCarlo et al., 2006; Drewnick et al., 2006). Detailed descriptions of the HR-ToF-AMS and the sampling site can be found elsewhere (Lee et al., 2015). For AMS measure-

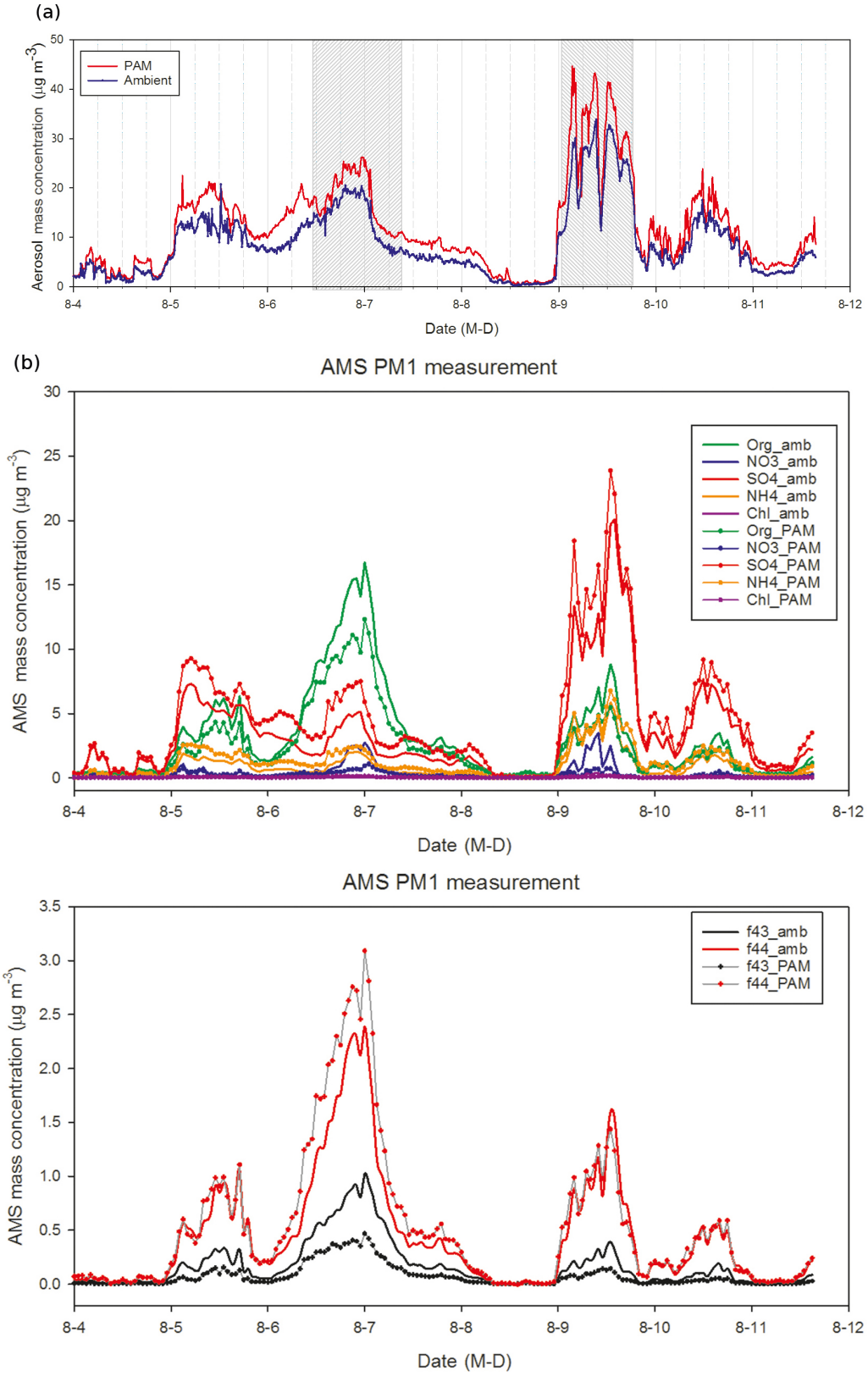
(a)
PAM
Ambient
Aerosol mass concentration (μg m-3)
Date (M-D)
(b)
AMS PM1 measurement
Org_amb
NO3_amb
SO4_amb
NH4_amb
Chl_amb
Org_PAM
NO3_PAM
SO4_PAM
NH4_PAM
Chl_PAM
AMS mass concentration (μg m-3)
Date (M-D)
AMS PM1 measurement
f43_amb
f44_amb
f43_PAM
f44_PAM
AMS mass concentration (μg m-3)
Date (M-D)

Figure 2.

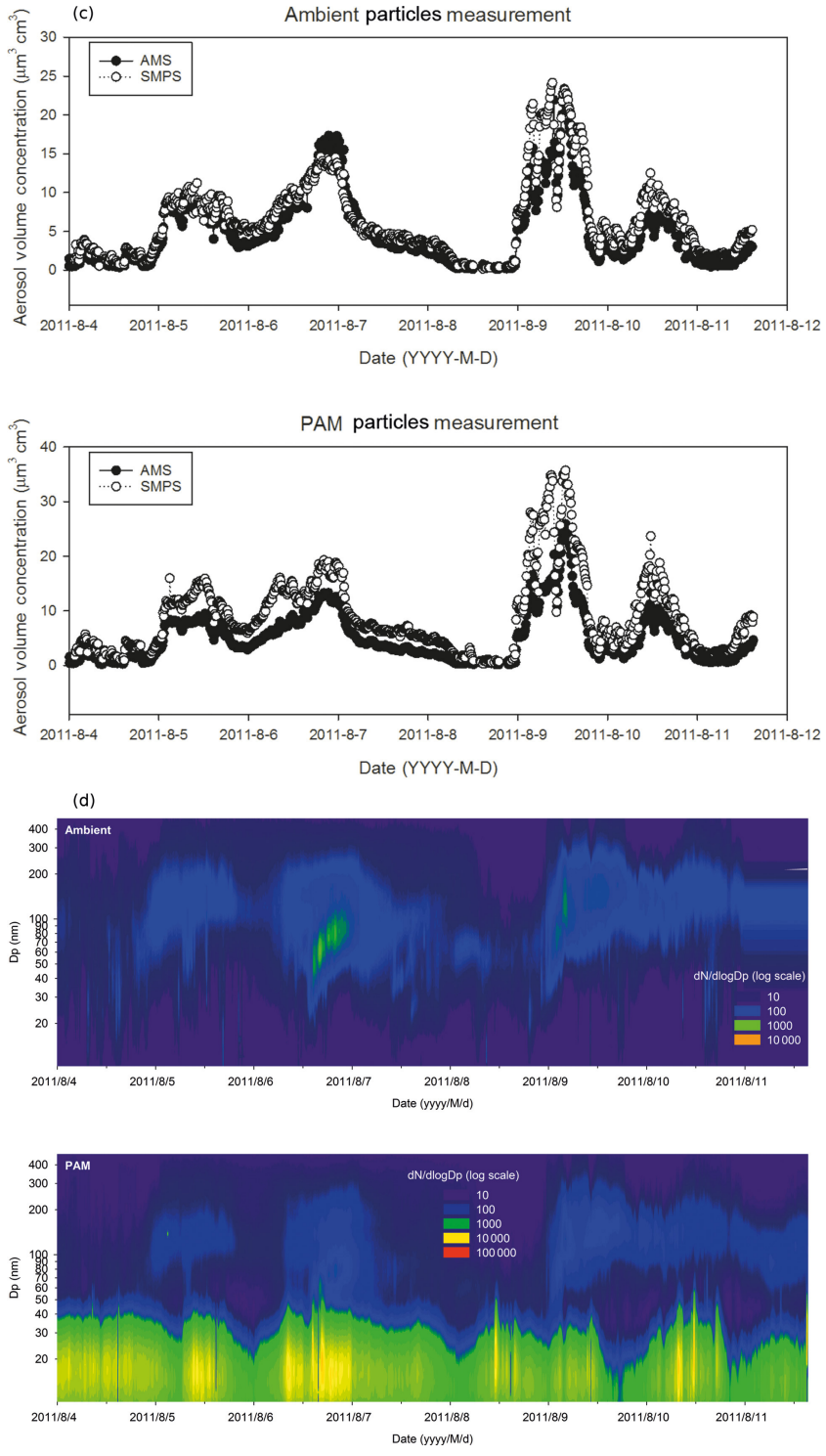

Figure 2. **(a)** Aerosol particle mass concentrations from SMPS measurements for ambient and PAM aerosols. **(b)** Mass concentrations of major components measured by HR-ToF-AMS including organics, nitrate, sulfate, ammonium, chloride, and m/z 43 and m/z 44. Solid lines and lines with markers represent ambient aerosol particles and PAM aerosol particles, respectively. Shaded periods represent the organics-dominated episode (6 August 11:00 LT to 7 August 09:00 LT) and the sulfate-dominated episode (9 August 01:00 LT to 9 August 14:00 LT). The lowest mass concentration observed on 8 August was due to rain. **(c)** Time series of particle volume concentration measured from AMS and SMPS. Particle volume concentration from AMS was calculated with mass concentration and composition-dependent density. **(d)** The size-separated number concentrations of ambient and PAM aerosol particles measured by SMPS.

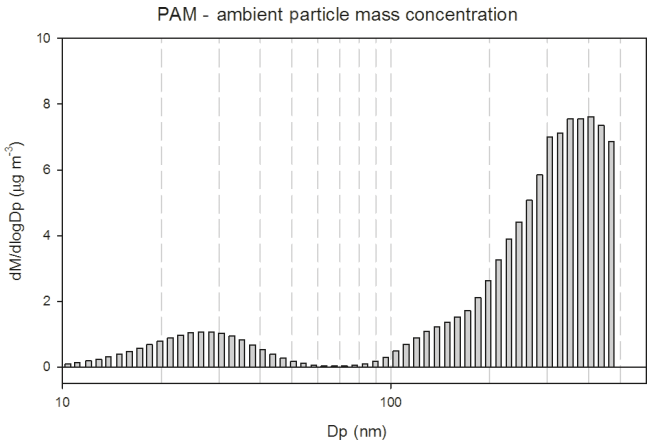

Figure 3. SMPS mass concentration difference between PAM and ambient aerosol particles averaged for the entire sampling period.

ments, a composition-dependent collection efficiency was applied by adopting the result of Middlebrook et al. (2012). Due to the detection range of the SMPS, the enhancement or loss of particles greater than 500 nm in diameter was not observed in SMPS measurements. The particle mass concentration from SMPS was obtained from the volume concentration multiplied by a fixed particle density of $1.4\,\mathrm{g\,cm^{-3}}$.

Some of the condensable gases formed in the PAM reactor do not contribute to the observed particle mass concentration sampled by the SMPS and AMS at the exit of the PAM reactor. Some are deposited on the PAM reactor walls, and some do not condense before the particles are sampled. The calculation of the condensation sink indicates the fraction that are measured as particles. These calculations indicate that typically 60 to 70 % of the condensable gases did condense on particles before the particles were measured (Fig. S5 in the Supplement). The particle mass concentrations shown in the results have been corrected for this loss and the details of the correction are described in the Supplement (Fig. S6). The resulting mass concentrations sampled through the PAM reactor and sampling system have an uncertainty of ±20 % (2σ confidence).

The overall mass spectra of organics indicate a substantial loss of less oxidized OA (e.g., m/z 41, 42, 43, ...) in the PAM reactor. In addition, the CO^+ and CO_2^+ groups increased and decreased in the PAM aerosol particles during these measurements. The terms m/z 43 and m/z 44 from the mass spectra correlate with less oxidized OA and further oxidized organics such as carboxylic acids, respectively. Therefore, the discussion of ions observed at m/z 43 and m/z 44 should be broadly applicable to these two classes of organic compounds.

Gas-phase ozone (O_3), nitrogen dioxide (NO_2), carbon monoxide (CO), and particle-phase elemental carbon (EC) and organic carbon (OC) were simultaneously measured, along with meteorological parameters (Table 1). The HYSPLIT backward trajectory model, which was developed by the National Oceanic and Atmospheric Administration (NOAA), was used to examine the history of the sampled air masses (Wang et al., 2009).

In this study, therefore, we examined how the air masses reaching Baengnyeong Island were further oxidized during the effective aging time of 4.6 days, which is consistent with transport time from China but slightly longer than the time of typical maximum SOA production from aging (Ortega et al., 2016) under an OH diel mean of 1.5×10^6 molecules $\mathrm{cm^{-3}}$.

3 Results

3.1 Measurement overview of ambient and PAM aerosols

$PM_{1.0}$ aerosol particle mass concentrations varied from 0.5 to $44\,\mu\mathrm{g\,m^{-3}}$ for both the PAM aerosol particles and the ambient aerosol particles (Fig. 2a) during the entire experiment period. Choi et al. (2016) reported AMS measurements ($PM_{1.0}$) made at the same site during March–April 2012 and November–December 2013, for which $PM_{1.0}$ varied from the detection limit to $\sim 100\,\mu\mathrm{g\,m^{-3}}$. These $PM_{1.0}$ concentrations were lower than those measured in Changdao, which is located in the Bohai Sea (Hu et al., 2013; Choi et al., 2016; Lee et al., 2015). The PAM particle mass concentration was generally greater than the ambient particle mass concentration.

Particle mass concentration distributions of the ambient and PAM aerosol particles were averaged for the entire experiment and their difference is presented in Fig. 3. In the PAM reactor, the formation of nucleation-mode particles was always observed (average $d\mathrm{N}/d\log D_\mathrm{p} = 2 \times 10^5\ \mathrm{cm^{-3}}$; see Fig. S9 in the Supplement), but their contribution to the total particle mass concentration was relatively insignificant due to their small sizes of less than 50 nm in diameter (D_p). In comparison, the mass concentration of PAM aerosol particles increased at sizes larger than 200 nm. The averaged particle mass concentration between 50 and 200 nm in diameter was enhanced in the PAM reactor for the sampling period (Fig. 3), but particles were either lost or produced in the PAM reactor depending on the history of the air masses (Figs. 5 and S9). The formation of nucleation-mode particles in the PAM reactor was also observed in previous studies (Kang et al., 2011b; Ortega et al., 2016; Palm et al., 2016). Major constituents including sulfate, organics, ammonium, and nitrate for both ambient and PAM particles are presented in Fig. 3. Sulfate and ammonium concentrations in the PAM reactor were mostly higher than or similar to those in the ambient air. In contrast, total organics and nitrate were mostly lower in the PAM aerosol particles than in ambient aerosol particles.

Previous studies show that SOA formation from VOCs, including semi- and intermediate-volatile compounds (SVOCs

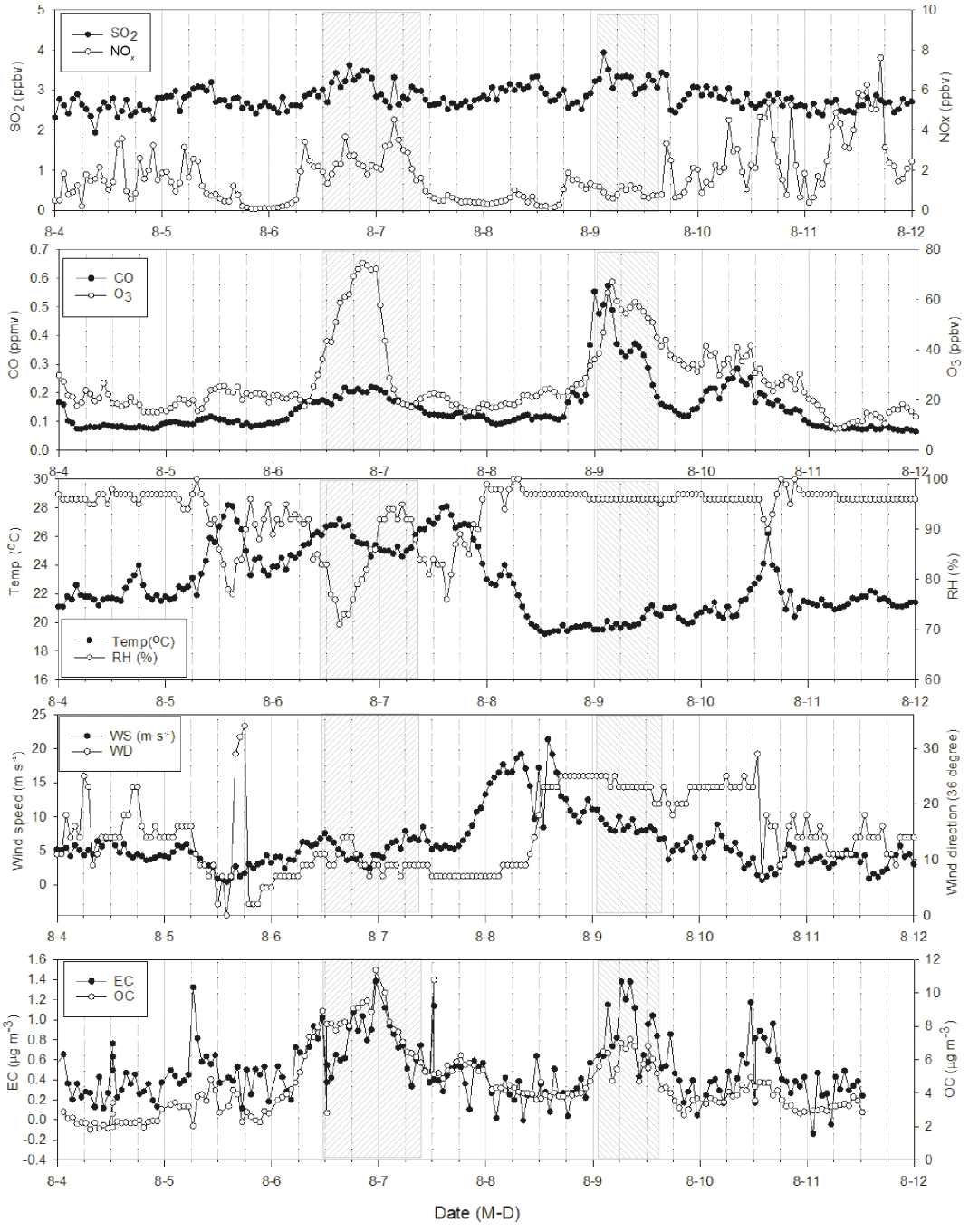

Figure 4. Hourly measurements of SO_2, NO_x, CO, O_3, EC, OC, and meteorological parameters for the entire sampling period.

and IVOCs), near the sources could be enhanced up to a few times greater than SOA from VOCs only (Hayes et al., 2015; Palm et al., 2016). It is possible that SVOCs and IVOCs could be lost to the reactor inlet plate and reactor wall due to their low saturation vapor pressures, leading to the underestimation of their contribution to SOA formation in the PAM reactor of this study. However, in our experiment, air masses had traveled at least 1 day from the Korean Peninsula or from east China before they were sampled in the PAM reactor. Thus, it is likely that SVOCs and IVOCs were already partitioned into the particle phase before the particles were sampled at the measurement station on Baengnyeong Island.

3.2 Organics- and sulfate-dominated episodes

Throughout the study, ambient aerosol particles were enhanced during two separate periods (shaded in Fig. 2a), with distinct differences in chemical composition between

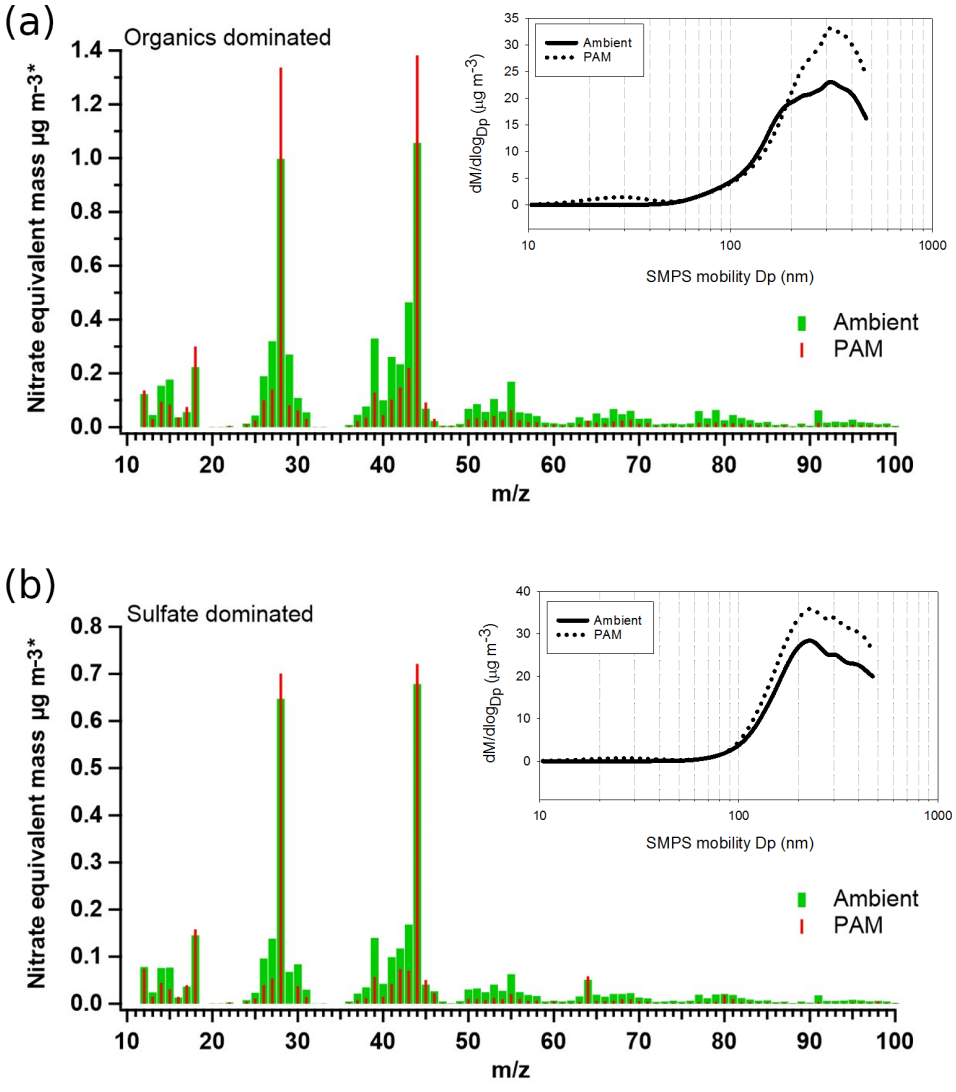

Figure 5. **(a)** AMS mass spectra of organics and SMPS mass size distribution averaged for the organics-dominated episode and **(b)** AMS mass spectra of organics and SMPS mass size distribution averaged for the sulfate-dominated episode.

the two. While the ambient air was enriched in organics during the first episode (6 August 11:00 LT to 7 August 09:00 LT), sulfate was dominant in the second episode (9 August 01:00 LT to 9 August 18:00 LT). During the two episodes, the levels of gaseous precursors including NO_x, SO_2, and CO were higher than in the remaining periods (Fig. 4). The ratios of both SO_2 / NO_x and OC / EC were higher and the ratio of O_3 / CO was lower for the first case.

These two cases were distinguished by the air mass backward trajectories (Fig. 1b). Air passing over the Korean Peninsula had higher concentrations of organics than sulfate during the first episode. For the second episode, the air mass backward trajectory indicates that the sulfate-dominated air had been transported from southeast China. In addition, the air mass trajectories imply that sulfate-dominated aerosols lingered over the Yellow Sea and were aged more than the organics-dominated aerosols.

In addition, the aerosol particles differed in terms of size distributions between the two episodes (Fig. 5 and Table 1). In the PAM reactor, the particle mass concentration increased for particles smaller than 50 nm and larger than 200 nm for both episodes. At a size between 50 and 200 nm, however, the mass concentration of PAM-processed particles increased during the sulfate-dominated episode but slightly decreased during the organics-dominated episode.

The difference between the AMS-measured particle mass concentration and SMPS-measured particle mass concentration was greater in the sulfate-dominated episode than in the organics-dominated episode (Table 1 and Fig. 2c). The disagreement is largely associated with AMS and SMPS measurement uncertainties. However, the role of elemental car-

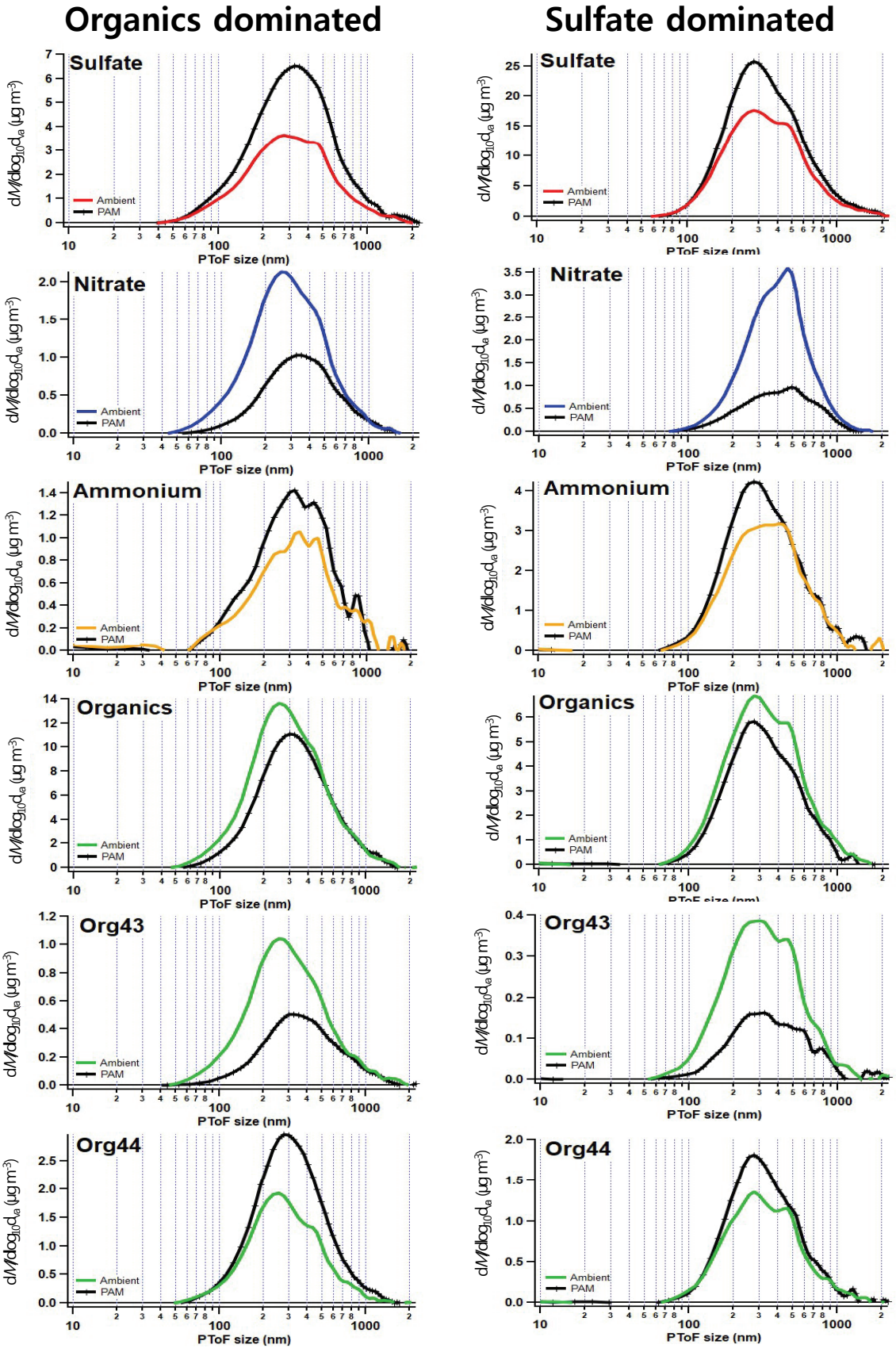

Figure 6. AMS PToF size distributions of PAM and ambient particle components averaged for each case.

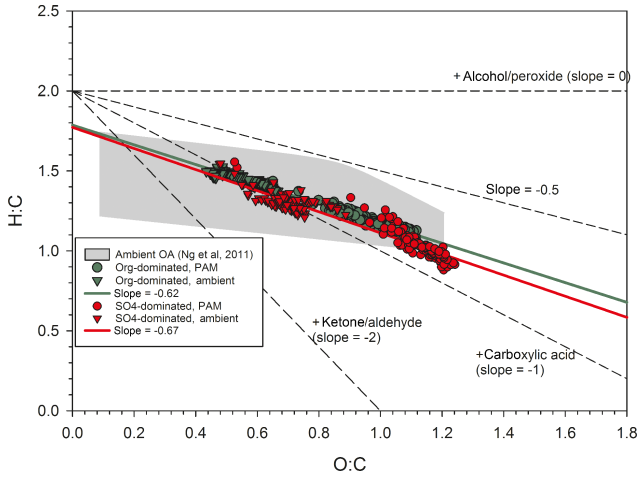

Figure 7. Van Krevelen diagram for two episodes. Dashed lines represent the van Krevelen slopes, Δ (H : C) / Δ (O : C), to show the direction of particular functional group additions (Heald et al., 2010). Shaded gray areas represent the H : C and O : C ranges observed in ambient OA (Ng et al., 2011).

bon or soil particles that are abundant in the study region (Lee et al., 2007; Lim et al., 2012) may not be ruled out because they are captured by SMPS but not by AMS.

The measurement results of size-separated chemical compositions provide detailed information on transformation processes in the PAM reactor. In general, aerosol particles in the PAM reactor experienced an increase in sulfate but a decrease in total organics and nitrate compared to the ambient aerosol particles (Fig. 6). The enhancement of sulfate in the PAM reactor was greater for the sulfate-dominated episode, and the reduction of organics in the PAM reactor was greater for the organics-dominated episode. The contribution of ammonium ions to the total mass concentration was also greatest when aerosol particles were enriched in sulfate. The m/z 43 decreased and m/z 44 increased in the PAM reactor for both episodes (Fig. 5).

Therefore, the following discussion is focused on these two distinct aerosols episodes. The size-separated chemical compositions are thoroughly examined and compared in order to elaborate on the formation of secondary aerosols and the evolution of ambient aerosols upon photooxidation in the PAM reactor.

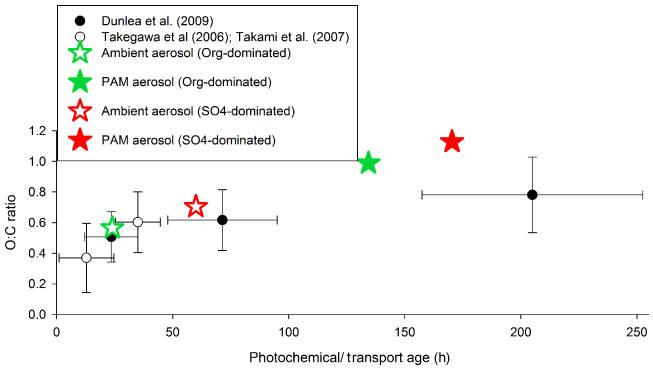

Figure 8. Comparison of O : C ratios in this study and other studies with respect to photochemical age. The photochemical ages in our measurements were obtained by the transport time calculated from a backward trajectory analysis and photochemical aging times in the PAM reactor. Other study data were obtained from Takegawa et al. (2006), Takami et al. (2007), and Dunlea et al. (2009).

4 Discussion

4.1 Nucleation of particles

In the current study, freshly nucleated particles ($D_p < 50$ nm) were always observed in the PAM reactor (Fig. 2d). In both cases, there was sufficient SO_2 and likely ammonia to nucleate new particles, but nucleation by extremely low-volatility organics cannot be ruled out. In previous field studies, increases in the mass concentration of PAM aerosol particles were dependent on the ambient SO_2 concentrations (Kang et al., 2013). Palm et al. (2016) also observed nucleation-mode particles being formed and competing for the role of condensation sink with preexisting accumulation-mode particles. The number concentrations of nucleation-mode particles in the PAM reactor in the organics-dominated episode were an order of magnitude greater than those in the sulfate-dominated episode, while the SO_2 mixing ratios were similar (details in Fig. S9 in the Supplement). This could be evidence for the nucleation of extremely low-volatility organic compounds called highly oxygenated molecules (HOMs; Tröstl et al., 2016). Chemical composition was not available for nucleation-mode particles due to an AMS cutoff size of 50 nm in the present study. VOC concentrations for ambient air were not determined.

4.2 Formation and evolution of organic aerosols

The SMPS mass size distributions highlight the size range of 100 ~ 200 nm, in which PAM particle mass concentration was reduced for the organics-dominated episode (Fig. 5). A previous study showed that less oxidized organic aerosols were found more often than more oxidized OA in particles smaller than 200 nm (Sun et al., 2012). In addition, the mass concentration of m/z 43 was higher in less oxidized OA than more oxidized OA (Sun et al., 2012). In

the present study, the contribution of m/z 43 to total organics was greater in the organics-dominated episode than in the sulfate-dominated episode, and the loss of organics in the PAM reactor was also greater in the organics-dominated episode. These results suggest that the less oxidized OA was more in the organics-dominated episode than in the sulfate-dominated episode. The ratios of O : C were lower for organics-dominated aerosol particles than those of sulfate-dominated aerosol particles (Fig. 7). These results for the particle composition are consistent with the air mass trajectories (Fig. 1b), which show that the organics-dominated air masses were relatively less aged than those of the sulfate-dominated episode (Jimenez et al., 2009; Ng et al., 2011).

The AMS measurement results indicate that total organics and the m/z 43 component were consistently reduced in the PAM reactor. Possible loss mechanisms are the deposition of aerosol particles on the chamber wall (McMurry and Grosjean, 1985; La et al., 2016) and fragmentation reactions from further photooxidation to form products with higher vapor pressure (Lambe et al., 2012). As described in Sect. 3, the condensable organics loss to the wall surface and by heterogeneous oxidation were calculated to be about $30 \sim 40$ %. Also, mass concentration loss due to temperature differences in the ambient air and in the PAM reactor are estimated to be minimal. For the entire experiment, the O : C ratios of PAM aerosol particles were greater than those of ambient aerosols, with O : C ratios corresponding to less oxidized OA and more oxidized OA (Zhu et al., 2018). Thus, a chemical transformation from low O : C to high O : C probably explains the organic mass loss.

Organics are known to be oxidized by OH undergoing functionalization and fragmentation. The pathway by which this occurs is determined by the oxidation state of the existing organic aerosol particles. Functionalization dominates in the early stage of oxidation, which increases total organics and m/z 43, while fragmentation dominates in the later stage of oxidation, reducing OA mass concentration (Jimenez et al., 2009; Kroll et al., 2009; Chacon-Madrid et al., 2010; Henry and Donahue, 2012; Lambe et al., 2012). For highly oxidized OA with O : C ratios greater than 0.4, fragmentation becomes especially dominant, resulting in OA mass concentration loss.

In this study, the measured O : C ratios of the ambient aerosol particles were greater than 0.4 for both episodes (Fig. 7), which indicates that the observed ambient organic aerosol particles were aged enough to be fragmented. Figure 7 also shows that PAM OA has a higher O : C ratio and lower H : C ratio than ambient aerosol particles and that the van Krevelen slope (Δ (H : C) / Δ (O : C)) of both episodes was about -0.6. In a laboratory PAM experiment, Lambe et al. (2012) observed a similar tendency and explained that as SOA oxidized, the van Krevelen slope changed from minor fragmentation of carbonyls, acids, and alcohol to major fragmentation of acids. In addition, Hu et al. (2016) demonstrated that fragmentation became an important pathway of OA oxidation at OH exposure greater than 10^{11} molecules cm^{-3} s. At OH exposure of 7×10^{11} molecules cm^{-3} s, they observed 20 % OA mass concentration loss by volatilization followed by the fragmentation of heterogeneous reaction products on the particles. In the present study, the OH-induced OA mass concentration loss in the PAM reactor was about 25 % and 28 % for the organics-dominated and sulfate-dominated episode, respectively, at our OH exposure of 7×10^{11} molecules cm^{-3} s (Table 1).

The m/z 44 mass concentration increased in PAM aerosol particles. In particular, the increase in m/z 44 mass concentration was associated with larger sizes than the m/z 43 mass concentration loss (Fig. 6). As mentioned above, m/z 43 mass concentration loss was significant for sizes less than 200 nm in the AMS measurement, but most of the increase in m/z 44 mass concentration was observed in the size greater than 200 nm. If particles grew in size by heterogeneous oxidation of carbonyls to carboxylic acids on preexisting particle surfaces, the mass concentration decrease in m/z 43 should also have been associated with an increase in the m/z 44 mass concentration by the addition of oxygen. For both episodes, m/z 43 reduction was associated with m/z 44 enhancement in the PAM reactor; however, the total organics mass concentration was decreased. This result implies that the observed loss of particle mass concentration was caused by heterogeneous oxidation, which resulted in fragmentation and evaporation. The oxidation of organics in the atmosphere can occur both in the gas phase and through heterogeneous reactions. The gas-phase reaction is tens of times faster than the heterogeneous reaction, being limited by diffusion to the particle surface (Lambe et al., 2012). In our experiment, it was not feasible to distinguish the gas-phase oxidation of semi-volatile organics in equilibrium with the particle phase from the heterogeneous oxidation of organics on the particle surface. The distributions of less oxidized organics such as carbonyl groups with a semi-volatile nature in the gaseous and particulate phases are controlled by the partitioning equilibrium between the two phases. In contrast, further oxidized organics such as organic acid groups with low volatility tend to preferentially remain in the particle phase (Ng et al., 2011). It is therefore quite likely that the gas-phase concentration of m/z 43-like compounds decreased by further oxidation in the PAM reactor, leading to the evaporation of organic m/z 43 in the particle phase to be re-equilibrated with the decreased concentration in the gas phase. On the other hand, m/z 44-like compounds were sufficiently less volatile, and thus they underwent little evaporation to the gas phase. During the ~ 100 s of the residence time in the PAM reactor, the gas-phase reactions would be more efficient than relatively slower heterogeneous oxidation, but as the semi-volatile SOA compounds are depleted, then heterogeneous oxidation becomes more important (Lambe et al., 2012).

It was also found in a previous study that the loss of OA mass concentration was less for highly oxidized OA than for less oxidized OA due to heterogeneous oxidation (Kessler et

al., 2012). In addition to the loss of less oxidized organics (m/z 43), the AMS measurements indicated that highly oxidized OA (m/z 44) were produced in the PAM reactor. In particular, the m/z 44 peak was found to occur in the same size range as that of sulfate. These results suggest that SOA is formed by gas-phase oxidation and subsequent condensation on the surface of existing sulfate particles. Indeed, robust evidence for this can be found in detailed laboratory studies of SOA formation on acidic seed particles (Jang et al., 2002, 2006; Kang et al., 2007).

This difference in behavior between the two episodes is consistent with the evolution of particle aging. The organics-dominated episode had particles that have been aged less and therefore contain less oxygenated molecules that can be further oxidized. The sulfate-dominated episode had more aged particles that were more depleted in semi-volatile organics so that further oxidation would need to proceed through heterogeneous oxidation even though it is slower than gas-phase oxidation.

4.3 Formation and evolution of inorganic aerosols

In the PAM aerosol particles, sulfate concentrations were always greater than or similar to those of the ambient aerosol particles for the entire experiment period. This increase is expected because ambient SO_2 was about 3 ppbv in both episodes and some of this SO_2 would be converted to sulfate and either nucleate or be deposited on existing particles in the PAM reactor (Kang et al., 2007). For the two selected episodes, sulfate mass concentration noticeably increased in accumulation mode (Fig. 6). Although nucleation-mode particles increased in number concentration to a great extent, their mass concentration contribution was small at the ambient level of gaseous precursors. In this study, the variation in ammonium concentrations was similar to that of sulfate (Fig. 2b). In addition, the equivalent ratios of sulfate and nitrate to ammonium indicated that the ambient particles were mostly acidic.

In the organics-dominated episode, the increase in the PAM aerosol particle mass concentrations for particles larger than 200 nm resulted from the formation of sulfate and m/z 44 as described earlier (Figs. 5 and 6); sulfate exhibited a broad peak in 200–500 nm particles, as in ambient particles. In comparison, the sulfate increase shifted toward smaller sizes in the 200–400 nm range during the sulfate-dominant episode, leading to a sharp peak at 200 nm. An increase in sulfate mass concentration was noticeable between 200 and 400 nm. A major inorganic constituent, nitrate, was lost in the PAM reactor during both episodes, with an ambient nitrate concentration that was comparable to the levels of sulfate and organics concentration (Fig. 2b). The nitrate concentration loss occurs in the PAM reactor because of the efficient conversion of SO_2 to sulfate, causing the particles to become acidic and causing particulate nitrate (HNO_3(p)) to evaporate. A plausible source of HNO_3(p) in the PAM reactor is the formation of gaseous HNO_3(g) and deposition on the particles. If a particle is acidic in the presence of sulfuric acids, nitrate easily evaporates back to the gas phase. As stated in Sect. 2, the loss of nitrate by temperature-induced evaporation would be insignificant.

In the organics-dominated episode, the normality balance of ammonium with sulfate and nitrate (sulfate + nitrate) [$\mu eq\,L^{-1}$] / ammonium [$\mu eq\,L^{-1}$] was 1.34 in ambient particles, which was reduced to 1.22 in PAM particles with enhanced sulfate and ammonium but with nitrate being lost (details in Fig. S8 in the Supplement). In the sulfate-dominated episode, the ammonium balance remained unchanged in PAM particles due to an equivalent loss of nitrate over the condensation mode with its mode being shifted toward larger size. These results illustrate the role of sulfate in determining the chemical compositions and mass loadings of aerosol particles in northeast Asia.

4.4 Atmospheric implications

The ambient OA in the present study was moderately to well aged, as indicated by their O : C ratios being greater than 0.4. OA was chemically and physically transformed in the PAM reactor, resulting in increased O : C ratios and decreased OA mass concentrations by photochemical oxidation and fragmentation processes. Although the oxidant levels of OH and O_3 in the PAM reactor far exceeded the ambient levels, the H : C and O : C ratios of the ambient and PAM OA were in close agreement with those observed in the atmosphere (Ng et al., 2011; Fig. 7). These results provide good evidence for the ability of the PAM reactor to accelerate oxidation processes in ambient air under high O_3 and OH conditions and to represent atmospheric aging of approximately 5 days without physical removal processes such as dry or wet deposition. It further confirms that the PAM reactor is applicable for field studies to observe the aging processes of various types of precursors and aerosols including emission sources and long-range-transported air masses.

The O : C ratios of OA from this study were plotted against aging time and compared with those observed in East Asia (Fig. 8), where the O : C ratios were found to increase with transport time across the Pacific Ocean (Takegawa et al., 2006; Takami et al., 2007; Dunlea et al., 2009). The O : C ratios of the bulk OA depend on the mass concentrations of organic constituents because the saturation vapor pressure varies with the molecular weight of the organics (Donahue et al., 2006). Thus, the O : C ratios from different studies are not directly comparable if their OA concentrations vary over a wide range. In Fig. 8, OA mass concentrations ranged up to 10 $\mu g\,m^{-3}$ and thus a comparison among different sets of measurements is suitable. In the real atmosphere, the fate and evolution of secondary aerosols could be affected by the scavenging of oxidized OA and inorganic aerosols on the cloud droplets by aqueous aerosol surface reaction (Dunlea et al., 2009), the nucleation of new particles due to the en-

trainment of free tropospheric air (Song et al., 2010), or dry deposition on the dust particles (Dunlea at al., 2009). It is noteworthy that the increase in O : C ratios with photochemical aging was slightly higher in our results than in those of previous studies, which is possibly due to the omission of these scavenging processes in the PAM reactor.

The results of this study imply that SO_2 plays a key role in increasing secondary aerosol concentrations in East Asia because the lifetime of SO_2 is longer than that of VOCs and because sulfate is relatively stable in the particle phase once formed, in contrast to nitrate and organics. While SOA formation is more important near sources or in fresh air masses, OA oxidation occurs continuously during the transport of air masses. The formation yield of sulfate from SO_2 is greater than that of organic aerosol particles during $3 \sim 4$ days of aging in the Asian pollution plume because of the fast depletion of SOA precursors (Dunlea et al., 2009), which is consistent with our results. In particular, this study indicates that relatively less aged OA was in equilibrium with the gas phase, through which the oxidation of less oxidized OA was carried out, leading to increased OA mass concentrations in the CCN size range (200–400 nm). The increased O : C ratios rendered particles more hygroscopic, thereby facilitating their activation as CCNs (Massoli et al., 2010). Thus, the climate effect of OA aging should be considered along with decreases in OA mass loading when transported across long distances.

Data availability. Measurement data and analysis results are available upon request from the corresponding author (meehye@korea.ac.kr).

The Supplement related to this article is available online at https://doi.org/10.5194/acp-18-6661-2018-supplement.

Competing interests. The authors declare that they have no conflict of interest.

Acknowledgements. This research was supported by the Basic Science Research Program through the National Research Foundation of Korea (NRF) funded by the Ministry of Science, Information, and Communications Technology & Future Planning (NRF-2017R1A2B4012143). Eunha Kang is especially thankful for support from the Basic Science Research Program through the National Research Foundation of Korea (NRF) funded by the Ministry of Education (NRF-2011-355-c00174).

Edited by: Sergey A. Nizkorodov
Reviewed by: two anonymous referees

References

Aggarwal, S. G. and Kawamura, K.: Carbonaceous and inorganic composition in long-range transported aerosols over northern Japan: Implication for aging of water-soluble organic fraction, Atmos. Environ., 43, 2532–2540, https://doi.org/10.1016/j.atmosenv.2009.02.032, 2009.

Brock, C. A., Hudson, P. K., Lovejoy, E. R., Sullivan, A., Nowak, J. B., Huey, L. G., Cooper, O. R., Cziczo, D. J., de Gouw, J., Fehsenfeld, F. C., Holloway, J. S., Hubler, G., Lafleur, B. G., Murphy, D. M., Neuman, J. A., Nicks, D. K., Orsini, D. A., Parrish, D. D., Ryerson, T. B., Tanner, D. J., Warneke, C., Weber, R. J., and Wilson, J. C.: Particle characteristics following cloud-modified transport from Asia to North America, J. Geophys. Res.-Atmos., 109, D23S26, https://doi.org/10.1029/2003jd004198, 2004.

Chacon-Madrid, H. J., Presto, A. A., and Donahue, N. M.: Functionalization vs. fragmentation: n-aldehyde oxidation mechanisms and secondary organic aerosol formation, Phys. Chem. Chem. Phys., 12, 13975–13982, https://doi.org/10.1039/C0cp00200c, 2010.

Choi, J., Kim, J., Lee, T., Choi, Y., Park, T., Oh, J., Park, J., Ahn, J., Jeon, H., Koo, Y., Kim, S., Hong, Y., and Hong, J.: A Study on Chemical Characteristics of Aerosol Composition at West Inflow Regions in the Korean Peninsula I. Characteristics of PM Concentration and Chemical Components, J. Korea Soc. Atmos. Environ., 32, 469–484, https://doi.org/10.5572/KOSAE.2016.32.5.469, 2016.

Cubison, M. J., Ortega, A. M., Hayes, P. L., Farmer, D. K., Day, D., Lechner, M. J., Brune, W. H., Apel, E., Diskin, G. S., Fisher, J. A., Fuelberg, H. E., Hecobian, A., Knapp, D. J., Mikoviny, T., Riemer, D., Sachse, G. W., Sessions, W., Weber, R. J., Weinheimer, A. J., Wisthaler, A., and Jimenez, J. L.: Effects of aging on organic aerosol from open biomass burning smoke in aircraft and laboratory studies, Atmos. Chem. Phys., 11, 12049–12064, https://doi.org/10.5194/acp-11-12049-2011, 2011.

Donahue, N. M., Robinson, A. L., Stanier, C. O., and Pandis, S. N.: Coupled partitioning, dilution, and chemical aging of semivolatile organics, Environ. Sci. Technol., 40, 2635–2643, https://doi.org/10.1021/Es052297c, 2006.

Dunlea, E. J., DeCarlo, P. F., Aiken, A. C., Kimmel, J. R., Peltier, R. E., Weber, R. J., Tomlinson, J., Collins, D. R., Shinozuka, Y., McNaughton, C. S., Howell, S. G., Clarke, A. D., Emmons, L. K., Apel, E. C., Pfister, G. G., van Donkelaar, A., Martin, R. V., Millet, D. B., Heald, C. L., and Jimenez, J. L.: Evolution of Asian aerosols during transpacific transport in INTEX-B, Atmos. Chem. Phys., 9, 7257–7287, https://doi.org/10.5194/acp-9-7257-2009, 2009.

Feiner, P., Brune, W., Miller, D., Zhang, L., Cohen, R., Romer, P., Goldstein, A., Keutsch, F., Skog, K., Wennberg, P., Nguyen, T., Teng, A., DeGouw, J., Koss, A., Wild, R., Brown, S., Guenther, A., Edgerton, E., Baumann, K., and Fry, J.: Testing Atmospheric Oxidation in an Alabama Forest, J. Atmos. Sci., 73, 4699–4710, https://doi.org/10.1175/JAS-D-16-0044.1, 2016.

George, I. J. and Abbatt, J. P. D.: Chemical evolution of secondary organic aerosol from OH-initiated heterogeneous oxidation, Atmos. Chem. Phys., 10, 5551–5563, https://doi.org/10.5194/acp-10-5551-2010, 2010.

Hallquist, M., Wenger, J. C., Baltensperger, U., Rudich, Y., Simpson, D., Claeys, M., Dommen, J., Donahue, N. M., George,

C., Goldstein, A. H., Hamilton, J. F., Herrmann, H., Hoffmann, T., Iinuma, Y., Jang, M., Jenkin, M. E., Jimenez, J. L., Kiendler-Scharr, A., Maenhaut, W., McFiggans, G., Mentel, Th. F., Monod, A., Prév[ˆo]t, A. S. H., Seinfeld, J. H., Surratt, J. D., Szmigielski, R., and Wildt, J.: The formation, properties and impact of secondary organic aerosol: current and emerging issues, Atmos. Chem. Phys., 9, 5155–5236, https://doi.org/10.5194/acp-9-5155-2009, 2009.

Hayes, P. L., Carlton, A. G., Baker, K. R., Ahmadov, R., Washenfelder, R. A., Alvarez, S., Rappenglück, B., Gilman, J. B., Kuster, W. C., de Gouw, J. A., Zotter, P., Prévôt, A. S. H., Szidat, S., Kleindienst, T. E., Offenberg, J. H., Ma, P. K., and Jimenez, J. L.: Modeling the formation and aging of secondary organic aerosols in Los Angeles during CalNex 2010, Atmos. Chem. Phys., 15, 5773–5801, https://doi.org/10.5194/acp-15-5773-2015, 2015.

Heald, C. L., Kroll, J. H., Jimenez, J. L., Docherty, K. S., DeCarlo, P. F., Aiken, A. C., Chen, Q., Martin, S. T., Farmer, D. K., and Artaxo, P.: A simplified description of the evolution of organic aerosol composition in the atmosphere, Geophys. Res. Lett., 37, L08803, https://doi.org/10.1029/2010gl042737, 2010.

Henry, K. M. and Donahue, N. M.: Photochemical Aging of alpha-Pinene Secondary Organic Aerosol: Effects of OH Radical Sources and Photolysis, J. Phys. Chem. A, 116, 5932–5940, https://doi.org/10.1021/Jp210288s, 2012.

Hu, W. W., Hu, M., Yuan, B., Jimenez, J. L., Tang, Q., Peng, J. F., Hu, W., Shao, M., Wang, M., Zeng, L. M., Wu, Y. S., Gong, Z. H., Huang, X. F., and He, L. Y.: Insights on organic aerosol aging and the influence of coal combustion at a regional receptor site of central eastern China, Atmos. Chem. Phys., 13, 10095–10112, https://doi.org/10.5194/acp-13-10095-2013, 2013.

Hu, W., Palm, B. B., Day, D. A., Campuzano-Jost, P., Krechmer, J. E., Peng, Z., de Sá, S. S., Martin, S. T., Alexander, M. L., Baumann, K., Hacker, L., Kiendler-Scharr, A., Koss, A. R., de Gouw, J. A., Goldstein, A. H., Seco, R., Sjostedt, S. J., Park, J.-H., Guenther, A. B., Kim, S., Canonaco, F., Prévôt, A. S. H., Brune, W. H., and Jimenez, J. L.: Volatility and lifetime against OH heterogeneous reaction of ambient isoprene-epoxydiols-derived secondary organic aerosol (IEPOX-SOA), Atmos. Chem. Phys., 16, 11563–11580, https://doi.org/10.5194/acp-16-11563-2016, 2016.

Huang, R. J., Zhang, Y., Bozzetti, C., Ho, K. F., Cao, J. J., Han, Y., Daellenbach, K. R., Slowik, J. G., Platt, S. M., Canonaco, F., Zotter, P., Wolf, R., Pieber, S. M., Bruns, E. A., Crippa, M., Ciarelli, G., Piazzalunga, A., Schwikowski, M., Abbaszade, G., Schnelle-Kreis, J., Zimmermann, R., An, Z., Szidat, S., Baltensperger, U., Haddad, I. E., and Prevot, A. S. H.: High secondary aerosol contribution to particulate pollution during haze events in China, Nature, 514, 218–222, https://doi.org/10.1038/nature13774, 2014.

Jang, M., Czoschke, N. M., Northcross, A. L., Cao, G., and Shaof, D.: SOA formation from partitioning and heterogeneous reactions: Model study in the presence of inorganic species, Environ. Sci. Technol., 40, 3013–3022, https://doi.org/10.1021/Es0511220, 2006.

Jang, M. S., Czoschke, N. M., Lee, S., and Kamens, R. M.: Heterogeneous atmospheric aerosol production by acid-catalyzed particle-phase reactions, Science, 298, 814–817, https://doi.org/10.1126/science.1075798, 2002.

Jimenez, J. L., Canagaratna, M. R., Donahue, N. M., Prevot, A. S. H., Zhang, Q., Kroll, J. H., DeCarlo, P. F., Allan, J. D., Coe, H., Ng, N. L., Aiken, A. C., Docherty, K. S., Ulbrich, I. M., Grieshop, A. P., Robinson, A. L., Duplissy, J., Smith, J. D., Wilson, K. R., Lanz, V. A., Hueglin, C., Sun, Y. L., Tian, J., Laaksonen, A., Raatikainen, T., Rautiainen, J., Vaattovaara, P., Ehn, M., Kulmala, M., Tomlinson, J. M., Collins, D. R., Cubison, M. J., Dunlea, E. J., Huffman, J. A., Onasch, T. B., Alfarra, M. R., Williams, P. I., Bower, K., Kondo, Y., Schneider, J., Drewnick, F., Borrmann, S., Weimer, S., Demerjian, K., Salcedo, D., Cottrell, L., Griffin, R., Takami, A., Miyoshi, T., Hatakeyama, S., Shimono, A., Sun, J. Y., Zhang, Y. M., Dzepina, K., Kimmel, J. R., Sueper, D., Jayne, J. T., Herndon, S. C., Trimborn, A. M., Williams, L. R., Wood, E. C., Middlebrook, A. M., Kolb, C. E., Baltensperger, U., and Worsnop, D. R.: Evolution of Organic Aerosols in the Atmosphere, Science, 326, 1525–1529, https://doi.org/10.1126/science.1180353, 2009.

Kang, E., Root, M. J., Toohey, D. W., and Brune, W. H.: Introducing the concept of Potential Aerosol Mass (PAM), Atmos. Chem. Phys., 7, 5727–5744, https://doi.org/10.5194/acp-7-5727-2007, 2007.

Kang, E., Brune, W. H., Kim, S., Yoon, S. C., Jung, M., and Lee, M.: A preliminary PAM measurement of ambient air at Gosan, Jeju to study the secondary aerosol forming potential, J. Korean Soc. Atmos. Environ., 27, 534–544, https://doi.org/10.5572/KOSAE.2011.27.5.534, 2011a.

Kang, E., Toohey, D. W., and Brune, W. H.: Dependence of SOA oxidation on organic aerosol mass concentration and OH exposure: experimental PAM chamber studies, Atmos. Chem. Phys., 11, 1837–1852, https://doi.org/10.5194/acp-11-1837-2011, 2011b.

Kang, E., Han, J., Lee, M., Lee, G., and Kim, J. C.: Chemical characteristics of size-resolved aerosols from Asian dust and haze episode in Seoul metropolitan city, Atmos. Res., 127, 34–46, https://doi.org/10.1016/j.atmosres.2013.02.002, 2013.

Kessler, S. H., Nah, T., Daumit, K. E., Smith, J. D., Leone, S. R., Kolb, C. E., Worsnop, D. R., Wilson, K. R., and Kroll, J. H.: OH-Initiated Heterogeneous Aging of Highly Oxidized Organic Aerosol, J. Phys. Chem. A, 116, 6358–6365, https://doi.org/10.1021/Jp212131m, 2012.

Kim, Y. J., Woo, J.-H., Ma, Y.-I., Kim, S., Nam, J. S., Sung, H., Choi, K.-C., Seo, J., Kim, J. S., Kang, C.-H., Lee, G., Ro, C.-U., Chang, D., and Sunwoo, Y.: Chemical characteristics of long-range transport aerosol at background sites in Korea, Atmos. Environ., 43, 5556–5566, https://doi.org/10.1016/j.atmosenv.2009.03.062, 2009.

King, S. M., Rosenoern, T., Shilling, J. E., Chen, Q., Wang, Z., Biskos, G., McKinney, K. A., Pöschl, U., and Martin, S. T.: Cloud droplet activation of mixed organic-sulfate particles produced by the photooxidation of isoprene, Atmos. Chem. Phys., 10, 3953–3964, https://doi.org/10.5194/acp-10-3953-2010, 2010.

Kroll, J. H. and Seinfeld, J. H.: Chemistry of secondary organic aerosol: Formation and evolution of low-volatility organics in the atmosphere, Atmos. Environ., 42, 3593–3624, https://doi.org/10.1016/j.atmosenv.2008.01.003, 2008.

Kroll, J. H., Smith, J. D., Che, D. L., Kessler, S. H., Worsnop, D. R., and Wilson, K. R.: Measurement of fragmentation and functionalization pathways in the heterogeneous oxidation of oxidized organic aerosol, Phys. Chem. Chem. Phys., 11, 8005–8014, https://doi.org/10.1039/B905289e, 2009.

La, Y. S., Camredon, M., Ziemann, P. J., Valorso, R., Matsunaga, A., Lannuque, V., Lee-Taylor, J., Hodzic, A., Madronich, S., and Aumont, B.: Impact of chamber wall loss of gaseous organic compounds on secondary organic aerosol formation: explicit modeling of SOA formation from alkane and alkene oxidation, Atmos. Chem. Phys., 16, 1417–1431, https://doi.org/10.5194/acp-16-1417-2016, 2016.

Lambe, A. T., Ahern, A. T., Williams, L. R., Slowik, J. G., Wong, J. P. S., Abbatt, J. P. D., Brune, W. H., Ng, N. L., Wright, J. P., Croasdale, D. R., Worsnop, D. R., Davidovits, P., and Onasch, T. B.: Characterization of aerosol photooxidation flow reactors: heterogeneous oxidation, secondary organic aerosol formation and cloud condensation nuclei activity measurements, Atmos. Meas. Tech., 4, 445–461, https://doi.org/10.5194/amt-4-445-2011, 2011.

Lambe, A. T., Onasch, T. B., Croasdale, D. R., Wright, J. P., Martin, A. T., Franklin, J. P., Massoli, P., Kroll, J. H., Canagaratna, M. R., Brune, W. H., Worsnop, D. R., and Davidovits, P.: Transitions from Functionalization to Fragmentation Reactions of Laboratory Secondary Organic Aerosol (SOA) Generated from the OH Oxidation of Alkane Precursors, Environ. Sci. Technol., 46, 5430–5437, https://doi.org/10.1021/Es300274t, 2012.

Lambe, A. T., Chhabra, P. S., Onasch, T. B., Brune, W. H., Hunter, J. F., Kroll, J. H., Cummings, M. J., Brogan, J. F., Parmar, Y., Worsnop, D. R., Kolb, C. E., and Davidovits, P.: Effect of oxidant concentration, exposure time, and seed particles on secondary organic aerosol chemical composition and yield, Atmos. Chem. Phys., 15, 3063–3075, https://doi.org/10.5194/acp-15-3063-2015, 2015.

Lee, J. D., Young, J. C., Read, K. A., Hamilton, J. F., Hopkins, J. R., Lewis, A. C., Bandy, B. J., Davey, J., Edwards, P., Ingham, T., Self, D. E., Smith, S. C., Pilling, M. J., and Self, D. E.: Measurement and calculation of OH reactivity at a United Kingdom coastal site, J. Atmos. Chem., 64, 53–76, https://doi.org/10.1007/s10874-010-9171-0, 2009.

Lee, M., Song, M., Moon, K. J., Han, J. S., Lee, G., and Kim, K. R.: Origins and chemical characteristics of fine aerosols during the northeastern Asia regional experiment (atmospheric brown cloud east Asia regional experiment 2005), J. Geophys. Res.-Atmos., 112, D22S29 https://doi.org/10.1029/2006jd008210, 2007.

Lee, T., Choi, J., Lee, G., Ahn, J., Park, J., Atwood, S. A., Schurman, M., Choi, Y., Chung, Y., and Collett Jr. J. L.: Characterization of Aerosol Composition, Concentrations, and Sources at Baengnyeong Island, Korea using an Aerosol Mass Spectrometer, Atmos. Environ., 120, 297–306, https://doi.org/10.1016/j.atmosenv.2015.08.038, 2015.

Li, Z., Li, C., Chen, H., Tsay, S. C., Holben, B., Huang, J., Li, B., Maring, H., Qian, Y., Shi, G., Xia, X., Yin, Y., Zheng, Y., and Zhuang, G.: East Asian studies of tropospheric aerosols and their impact on regional climate (EAST-AIRC): An overview, J. Geophys. Res., 116, D00L34, https://doi.org/10.1029/2010JD015257, 2011.

Lim, S., Lee, M., Lee, G., Kim, S., Yoon, S., and Kang, K.: Ionic and carbonaceous compositions of PM_{10}, $PM_{2.5}$ and $PM_{1.0}$ at Gosan ABC Superstation and their ratios as source signature, Atmos. Chem. Phys., 12, 2007–2024, https://doi.org/10.5194/acp-12-2007-2012, 2012.

Lim, S., Lee, M., Kim, S.-W., Yoon, S.-C., Lee, G., and Lee, Y. J.: Absorption and scattering properties of organic carbon versus sulfate dominant aerosols at Gosan climate observatory in Northeast Asia, Atmos. Chem. Phys., 14, 7781–7793, https://doi.org/10.5194/acp-14-7781-2014, 2014.

Link, M. F., Kim, J., Park, G., Lee, T., Park, T., Babar, Z. B., Sung, K., Kim, P., Kang, W., Kim, J., Choi, Y., Son, J., Lim, H.-J., and Farmer, D. K.: Elevated production of NH_4NO_3 from the photochemical processing of vehicle exhaust: Implications for air quality in the Seoul Metropolitan Region, Atmos. Environ., 156, 95–101, https://doi.org/10.1016/j.atmosenv.2017.02.031, 2017.

Mao, J., Ren, X., Chen, S., Brune, W. H., Chen, Z., Martinez, M., Harder, H., Lefer, B., Rappenglueck, B., Flynn, J., and Leuchner, M.,: Atmospheric oxidation capacity in the summer of Houston 2006: Comparison with summer measurements in other metropolitan studies, Atmos. Environ., 44, 4107–4115, https://doi.org/10.1016/j.atmosenv.2009.01.013, 2010.

Massoli, P., Lambe, A. T., Ahern, A. T., Williams, L. R., Ehn, M., Mikkila, J., Canagaratna, M. R., Brune, W. H., Onasch, T. B., Jayne, J. T., Petaja, T., Kulmala, M., Laaksonen, A., Kolb, C. E., Davidovits, P., and Worsnop, D. R.: Relationship between aerosol oxidation level and hygroscopic properties of laboratory generated secondary organic aerosol (SOA) particles, Geophys. Res. Lett., 37, L24801, https://doi.org/10.1029/2010gl045258, 2010.

McMurry, P. H. and Grosjean, D.: Gas and aerosol wall losses in Teflon film smog chambers, Environ. Sci. Technol., 19, 1176–1182, https://doi.org/10.1021/es00142a006, 1985.

Middlebrook, A. M., Bahreini, R., Jimenez, J. L., and Canagaratna, M. R.: Evaluation of Composition-Dependent Collection Efficiencies for the Aerodyne Aerosol Mass Spectrometer using Field Data. Aerosol Sci. Technol., 46, 258–271, https://doi.org/10.1080/02786826.2011.620041, 2012.

Morgan, W. T., Allan, J. D., Bower, K. N., Esselborn, M., Harris, B., Henzing, J. S., Highwood, E. J., Kiendler-Scharr, A., McMeeking, G. R., Mensah, A. A., Northway, M. J., Osborne, S., Williams, P. I., Krejci, R., and Coe, H.: Enhancement of the aerosol direct radiative effect by semi-volatile aerosol components: airborne measurements in North-Western Europe, Atmos. Chem. Phys., 10, 8151–8171, https://doi.org/10.5194/acp-10-8151-2010, 2010.

Ng, N. L., Canagaratna, M. R., Zhang, Q., Jimenez, J. L., Tian, J., Ulbrich, I. M., Kroll, J. H., Docherty, K. S., Chhabra, P. S., Bahreini, R., Murphy, S. M., Seinfeld, J. H., Hildebrandt, L., Donahue, N. M., DeCarlo, P. F., Lanz, V. A., Prévôt, A. S. H., Dinar, E., Rudich, Y., and Worsnop, D. R.: Organic aerosol components observed in Northern Hemispheric datasets from Aerosol Mass Spectrometry, Atmos. Chem. Phys., 10, 4625–4641, https://doi.org/10.5194/acp-10-4625-2010, 2010.

Ng, N. L., Canagaratna, M. R., Jimenez, J. L., Chhabra, P. S., Seinfeld, J. H., and Worsnop, D. R.: Changes in organic aerosol composition with aging inferred from aerosol mass spectra, Atmos. Chem. Phys., 11, 6465–6474, https://doi.org/10.5194/acp-11-6465-2011, 2011.

Ortega, A. M., Day, D. A., Cubison, M. J., Brune, W. H., Bon, D., de Gouw, J. A., and Jimenez, J. L.: Secondary organic aerosol formation and primary organic aerosol oxidation from biomass-burning smoke in a flow reactor during FLAME-3, Atmos. Chem. Phys., 13, 11551–11571, https://doi.org/10.5194/acp-13-11551-2013, 2013.

Ortega, A. M., Hayes, P. L., Peng, Z., Palm, B. B., Hu, W., Day, D. A., Li, R., Cubison, M. J., Brune, W. H., Graus, M., Warneke, C., Gilman, J. B., Kuster, W. C., de Gouw, J., Gutiérrez-Montes, C., and Jimenez, J. L.: Real-time measurements of secondary organic aerosol formation and aging from ambient air in an oxidation flow reactor in the Los Angeles area, Atmos. Chem. Phys., 16, 7411–7433, https://doi.org/10.5194/acp-16-7411-2016, 2016.

Palm, B. B., Campuzano-Jost, P., Ortega, A. M., Day, D. A., Kaser, L., Jud, W., Karl, T., Hansel, A., Hunter, J. F., Cross, E. S., Kroll, J. H., Peng, Z., Brune, W. H., and Jimenez, J. L.: In situ secondary organic aerosol formation from ambient pine forest air using an oxidation flow reactor, Atmos. Chem. Phys., 16, 2943–2970, https://doi.org/10.5194/acp-16-2943-2016, 2016.

Palm, B. B., Campuzano-Jost, P., Day, D. A., Ortega, A. M., Fry, J. L., Brown, S. S., Zarzana, K. J., Dube, W., Wagner, N. L., Draper, D. C., Kaser, L., Jud, W., Karl, T., Hansel, A., Gutiérrez-Montes, C., and Jimenez, J. L.: Secondary organic aerosol formation from in situ OH, O_3, and NO_3 oxidation of ambient forest air in an oxidation flow reactor, Atmos. Chem. Phys., 17, 5331–5354, https://doi.org/10.5194/acp-17-5331-2017, 2017.

Peng, Z., Day, D. A., Stark, H., Li, R., Lee-Taylor, J., Palm, B. B., Brune, W. H., and Jimenez, J. L.: HO_x radical chemistry in oxidation flow reactors with low-pressure mercury lamps systematically examined by modeling, Atmos. Meas. Tech., 8, 4863–4890, https://doi.org/10.5194/amt-8-4863-2015, 2015.

Peng, Z., Day, D. A., Ortega, A. M., Palm, B. B., Hu, W., Stark, H., Li, R., Tsigaridis, K., Brune, W. H., and Jimenez, J. L.: Non-OH chemistry in oxidation flow reactors for the study of atmospheric chemistry systematically examined by modeling, Atmos. Chem. Phys., 16, 4283–4305, https://doi.org/10.5194/acp-16-4283-2016, 2016.

Peltier, R. E., Hecobian, A. H., Weber, R. J., Stohl, A., Atlas, E. L., Riemer, D. D., Blake, D. R., Apel, E., Campos, T., and Karl, T.: Investigating the sources and atmospheric processing of fine particles from Asia and the Northwestern United States measured during INTEX B, Atmos. Chem. Phys., 8, 1835–1853, https://doi.org/10.5194/acp-8-1835-2008, 2008.

Ramana, M. V., Ramanathan, V., Feng, Y., Yoon, S. C., Kim, S. W., Carmichael, G. R., and Schauer, J. J.: Warming influenced by the ratio of black carbon to sulfate and the black-carbon source, Nat. Geosci., 3, 542–545, https://doi.org/10.1038/Ngeo918, 2010.

Song, M., Lee, M., Kim, J. H., Yum, S. S., Lee, G., and Kim, K.-R.: New particle formation and growth in relation to vertical mixing and chemical species during ABC-EAREX2005, Atmos. Res., 97, 359–370, https://doi.org/10.1016/j.atmosres.2010.04.013, 2010.

Sun, Y. L., Zhang, Q., Schwab, J. J., Yang, T., Ng, N. L., and Demerjian, K. L.: Factor analysis of combined organic and inorganic aerosol mass spectra from high resolution aerosol mass spectrometer measurements, Atmos. Chem. Phys., 12, 8537–8551, https://doi.org/10.5194/acp-12-8537-2012, 2012.

Takami, A., Miyoshi, T., Shimono, A., Kaneyasu, N., Kato, S., Kajii, Y., and Hatakeyama, S.: Transport of anthropogenic aerosols from Asia and subsequent chemical transformation, J. Geophys. Res.-Atmos., 112, D22S31, https://doi.org/10.1029/2006jd008120, 2007.

Takegawa, N., Miyakawa, T., Kondo, Y., Jimenez, J. L., Zhang, Q., Worsnop, D. R., and Fukuda, M.: Seasonal and diurnal variations of submicron organic aerosol in Tokyo observed using the Aerodyne aerosol mass spectrometer, J. Geophys. Res.-Atmos., 111, D11206, https://doi.org/10.1029/2005jd006515, 2006.

Timonen, H., Karjalainen, P., Saukko, E., Saarikoski, S., Aakko-Saksa, P., Simonen, P., Murtonen, T., Dal Maso, M., Kuuluvainen, H., Bloss, M., Ahlberg, E., Svenningsson, B., Pagels, J., Brune, W. H., Keskinen, J., Worsnop, D. R., Hillamo, R., and Rönkkö, T.: Influence of fuel ethanol content on primary emissions and secondary aerosol formation potential for a modern flex-fuel gasoline vehicle, Atmos. Chem. Phys., 17, 5311–5329, https://doi.org/10.5194/acp-17-5311-2017, 2017.

Tröstl, J., Chuang, W. K., Gordon, H., Heinritzi, M., Yan, C., Moltini, U., Ahlm, L., Frege, C., Bianchi, F., Wagner, R., Simon, M., Lehtipalo, K., Willaimson, C., Craven, J. S., Duplissy, J., Adamov, A., Almeida, J., Bernhammer, A.-K., Breitenlechner, M., Brilke, S., Dias, A., Ehrhart, S., Flagan, R., Franchin, A., Fuchs, C., Guida, R., Gysel, M., Hansel, A., Hoyle, C. R., Jokinen, T., Junninen, H., Kangasluoma, J., Keskinen, H., Kim, J., Krapf, M., Küsten, A., Laaksonen, A., Lawler, M., Keiminger, M., Mathot, S., Möhler, O., Nieminen, T., Onnela, A., Petäjä, T., Piel, F. M., Miettinen, P., Rissanen, M. P., Rondo, L., Sarnela, M., Schobesberger, S., Sengupta, K., Sipilä, M., Smith, J. N., Steiner, G., Tomè, A., Virtanen, A., Wagner, A. C., Weingartner, E., Wimmer, D., Winkler, P., Ye, P., Carslaw, K. S., Curtius, J., Dommen, J., Kirkby, J., Kulmala, M., Riipinen, I., Worsnop, D. R., Donahue, N. M., and Baltensperger, U.: The role of low-volatility organic compounds in initial particle growth in the atmosphere, Nature, 533, 527–531, https://doi.org/10.1038/nature18271, 2016.

Wang, Y. Q., Zhang, X. Y., and Draxler, R. R.: TrajStat: GIS-based software that uses various trajectory statistical analysis methods to identify potential sources from long-term air pollution measurement data, Environ. Modell. Softw. 24, 938–939, 2009.

Wu, Z. J., Cheng, Y. F., Hu, M., Wehner, B., Sugimoto, N., and Wiedensohler, A.: Dust events in Beijing, China (2004–2006): comparison of ground-based measurements with columnar integrated observations, Atmos. Chem. Phys., 9, 6915–6932, https://doi.org/10.5194/acp-9-6915-2009, 2009.

Zhang, J., Wang, Y., Huang, X., Liu, Z., Ji, D., and Sun, Y.: Characterization of organic aerosols in Beijing using an aerodyne high-resolution aerosol mass spectrometer, Adv. Atmos. Sci., 32, 877–888, https://doi.org/10.1007/s00376-014-4153-9, 2015.

Zhu, Q., Huang, X.-F., Cao, L.-M., Wei, L.-T., Zhang, B., He, L.-Y., Elser, M., Canonaco, F., Slowik, J. G., Bozzetti, C., El-Haddad, I., and Prévôt, A. S. H.: Improved source apportionment of organic aerosols in complex urban air pollution using the multilinear engine (ME-2), Atmos. Meas. Tech., 11, 1049–1060, https://doi.org/10.5194/amt-11-1049-2018, 2018.